Supplementary Material for

Evidence for fluid and melt generation in response to an asthenospheric upwelling beneath the Hangai Dome, Mongolia

Submitted to

Earth and Planetary Science Letters

Contents of this file

Introduction

Here we include additional explanatory details on the dimensionality analysis carried out on the magnetotelluric data, the 2-D inversion data fit and feature testing, additional information about the crustal melt fraction analysis and calculations, and an enlarged crustal section.

Text S1. Dimensionality analysis

Dimensionality analysis determines if a 2-D or 3-D resistivity model is needed to interpret the measured MT data. For 2-D data, tensor decomposition can be used to estimate the geo-electric strike direction (e.g., *McNeice and Jones*, 2001; *Chave and Jones*, 2012). Tensor decomposition was implemented on a site-by-site basis, which allows for a different strike angle to be computed at each site and each frequency. At short periods (< 1 s), there is no well-defined strike direction because the electromagnetic signals are only sampling the near surface resistivity structure, which is approximately 1-D or is controlled by very local structures. At longer periods (> 1 s) the MT signals sample deeper in the Earth and a well-defined regional strike direction of N105°E was observed (**Figure S1**). Phase tensor analysis was used to verify this result (e.g., *Booker,* 2014; *Chave and Jones*, 2012). It should be noted that the strike directions determined have an inherent 90° ambiguity. Therefore one direction must be chosen based on additional knowledge.
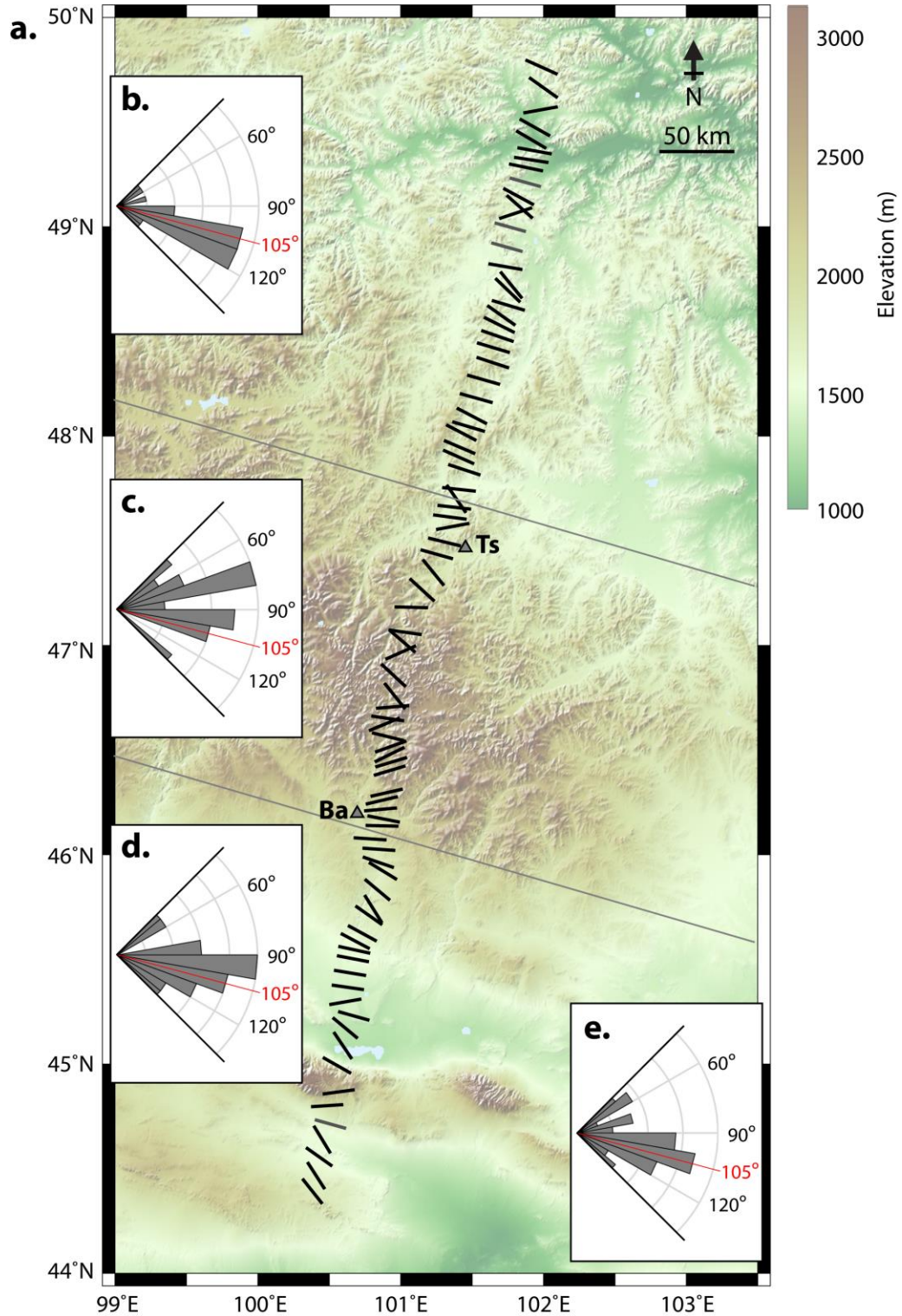
Figure S1: Strike analysis results using the tensor decomposition method, in map view (**a**) and as rose diagrams, for each segment (North (**b**), Central (**c**), South (**d**)) and overall (**e**), for 1 - 1000 s. Ts = Tsetserleg; Ba = Bayankhongor. A fairly consistent strike direction is seen over the whole Hangai region, although there is scatter in the central region, across the Hangai Dome, indicating complex structure. Overall, a strike direction of N105°E (red line) fits most of the data.

To determine the suitability of a unique geo-electric strike direction for all MT sites the strike direction was set to a given angle and the misfit from the tensor decomposition was determined for all sites and all periods. The misfit was calculated with a root mean squared (RMS) misfit between the 2-D MT impedance values predicted by the tensor decomposition method and the measured MT values (using an error floor of 3%). When the strike direction was varied from N90°E to N180°E, a clear minimum misfit was observed at a strike angle of N105°E (**Figure S2a**). However this does not fully describe how well all the data are fit. When the strike angle was set to the preferred direction of N105°E the misfit varied along the profile (**Figure S2b**). However, the generally low misfit values (< 2) indicate that a 2-D approach is valid. Some areas with higher misfits (i.e., red colors) may be due to 3-D effects.
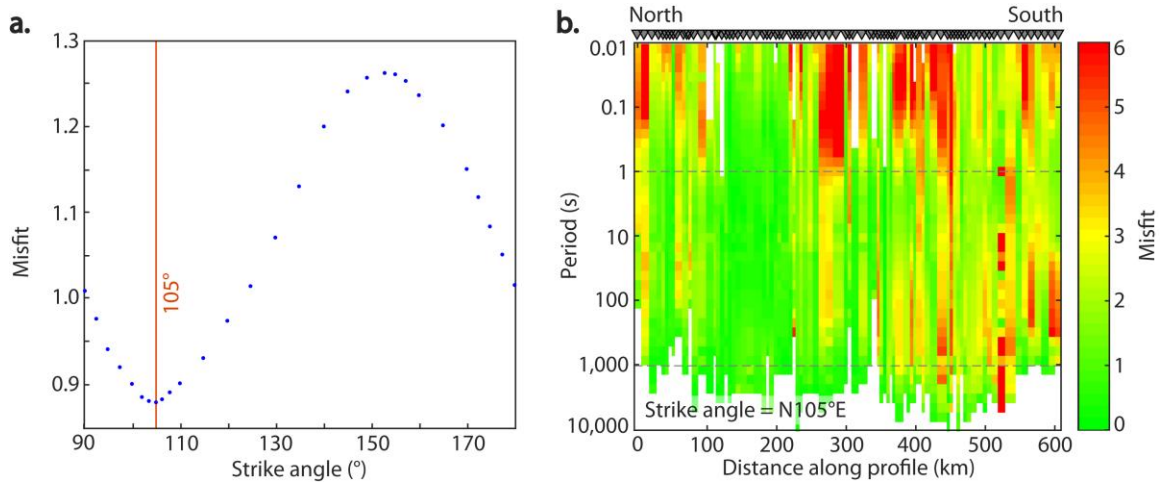

Figure S2: a: Fit from the tensor decomposition method for various strike directions, measured clockwise from North (i.e., East to South). The minima shows the preferred strike direction of N105°E (i.e., ESE). **b:** Pseudosection of the misfit from the tensor decomposition method, when a strike direction of N105°E is used for all sites. This analysis can be used to determine whether a single strike direction reasonably fits the data for all sites and all periods. Some areas (i.e., red colors) are distorted and may be better fit by a 3-D analysis. The period range of 1 – 1000 s is shown with dashed grey lines.

The phase tensor method can give information on dimensionality (and geo-electric strike direction) without imposing a priori the condition of two-dimensionality (*Chave and Jones*, 2012). Furthermore, the phase tensor is not affected by galvanic distortions (e.g., static shift effect). The phase tensors can be plotted in pseudo-section view as ellipses (**Figure S3a**) and colored with their phase-tensor skew value (ψ) (*Booker*, 2014; *Chave and Jones*, 2012). Note that the skew ψ is twice as large as the skew β (*Booker*, 2014). They will appear as a circle for a 1-D Earth environment and as an ellipse for a 2-D or 3-D Earth environment. Skew values for a perfect 2-D Earth equal 0° (blue colors) whereas skew values above ~6° (yellow to red colors) indicate that distortion and/or 3-D effects are significant. The phase tensor analysis establishes that a 2-D assumption is valid for the profile as a whole (**Figure S3b**). However, it is clear that certain regions of the profile display distortion and/or local 3-D resistivity structure, specifically the central region of the profile and the southern portion of the profile.
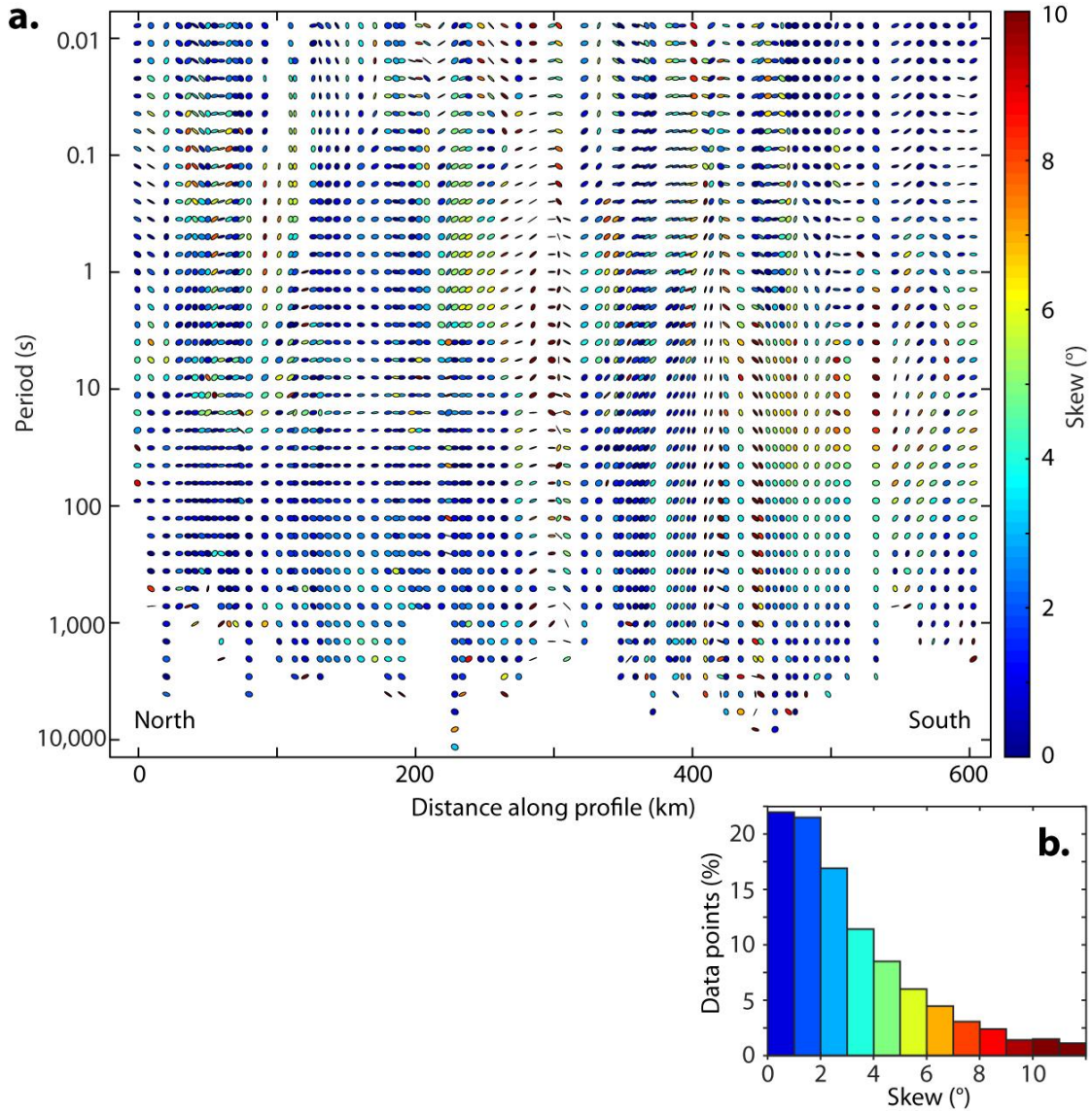

Figure S3: a: Phase tensor ellipses for all periods and all sites plotted along the profile and coloured with their skew values (ψ). High skew values (yellow to red colours) indicate significant distortion and/or 3-D effects. **b:** A histogram of skew values illustrates that most data points have skew < 6°.

Text S2. 2-D inversion data fit

The 2-D inversion was repeated for a wide range of model regularization parameters, using a gradient model penalty, and an appropriate regularization parameter was chosen as a compromise between closely fitting the measured MT data and producing a spatially smooth model. A representative fit of the model to the MT data at several sites can be seen in **Figure S4**. The total RMS misfit at each site is plotted in **Figure S5**.
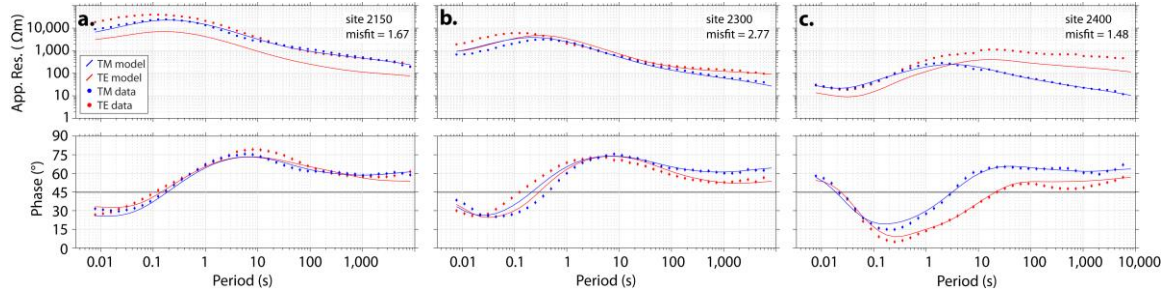

Figure S4: Characteristic data fit for the resistivity model at several MT sites from the northern region (**a**), the central Hangai region (**b**), and the southern region (**c**). The site in (**a**) shows a static shift effect which has been overcome by the inversion algorithm with little negative effect on the misfit. The site in (**b**) illustrates the difficulty in fitting the short-period data (< 1 s), which increases the overall misfit, but that an overall higher misfit (i.e. 2.77) can still fit the main features well. The site in (**c**) demonstrates the distinctly different data seen in the southern region.
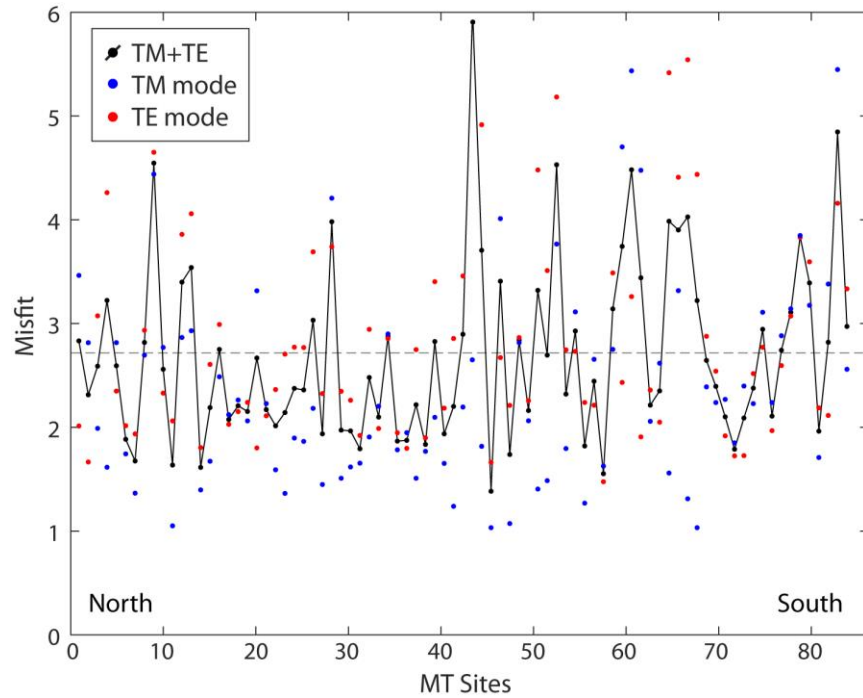

Figure S5: Misfit for each MT site of the 2-D resistivity model. A misfit of 1.0 implies that the model fits within the specified error (TM mode: error floor of 1.4° on phase and 10% on apparent resistivity; TE mode: error floor of 1.4° on phase and 100% on apparent resistivity). The model has a total misfit of 2.75 (dashed line). Dots show the misfit computed for TM mode only (blue; total = 2.37) and TE mode only (red; total = 2.94).

6

Many combinations of inversion parameters were investigated, and the final model generated (presented in Figure 3) is representative of most cases. The robustness of model features were tested in several ways, and one example is described here. The feature C3 and the deeper sub-lithospheric structure are mostly located below a strong crustal conductor (C2) which acts to limit the resolution below it. Therefore, we display a requirement test for the feature C3 (**Figure S6**).

When the feature was removed, by replacing it and everything below 100 Ωm (approximately everything below 70 km depth) with 100 Ωm (the starting model resistivity), the misfit increased from 2.75 to 3.33, indicating a worse fit to the MT data without this feature (**Figure S6b**). The inversion was then re-started and it was observed that the feature was re-introduced, in order to better fit the MT data, and that the misfit decreased to 2.88 (**Figure S6c**). This test illustrated that the feature is required. However, it also showed that the geometry of the upper mantle conductor C3 is not well-constrained, and can vary. The data can be nearly well fit (difference in RMS misfit of ~5%) by a slightly narrower, isolated anomaly or by a wider, doming anomaly, at the same location. None of these variations affect the interpretation of the model.
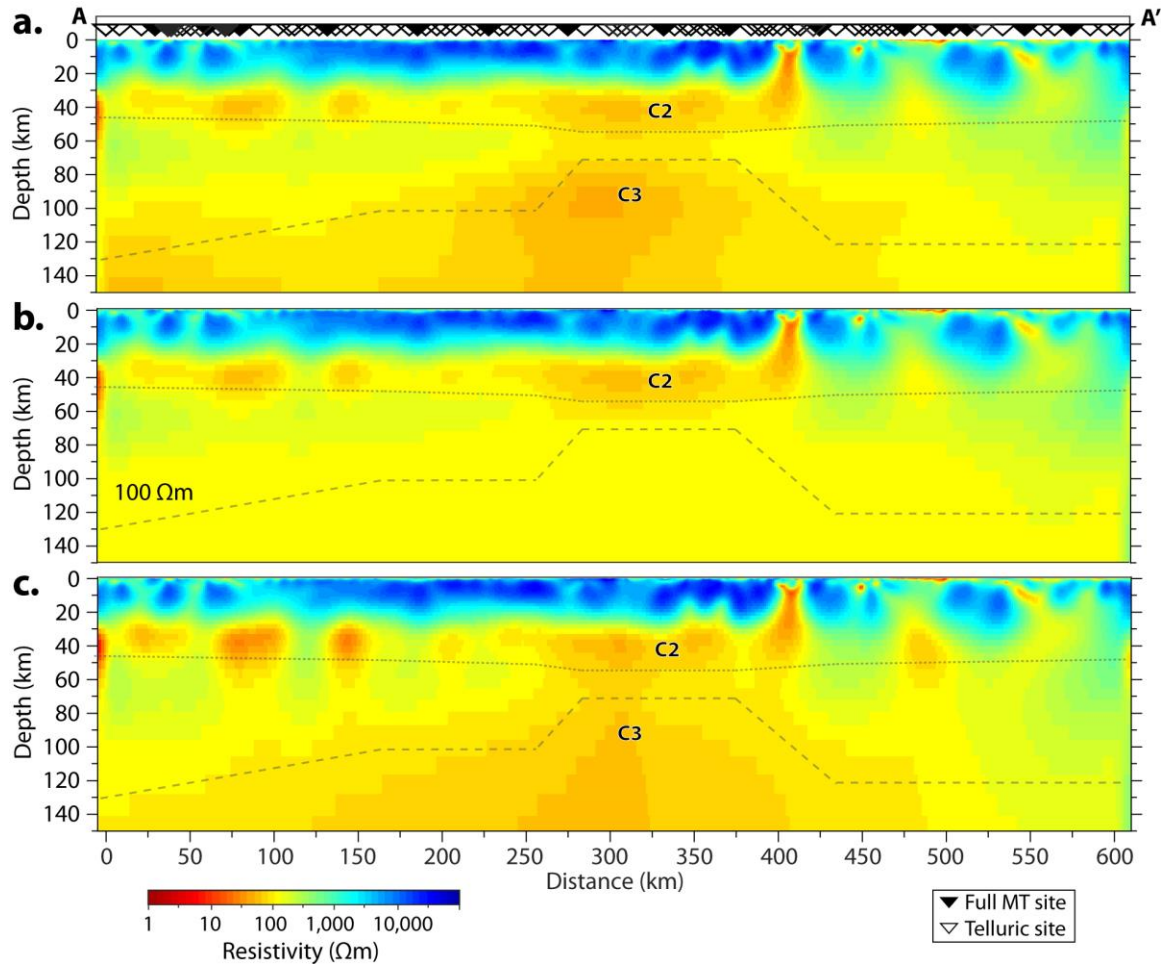

Figure S6: A test for the requirement of the feature C3. The 2-D inversion model (**a**) is edited to remove the feature (**b**), and the subsequent inversion using this as the prior model returns the feature (**c**). The recovered feature is required by the inversion in order to fit the MT data.

Text S3. Melt fraction analysis and calculations

If the low-resistivity anomalies detected are due to partial melt alone the minimum required melt fraction can be determined, as described in section 3.5.

Firstly, pure melt resistivity is computed. This is achieved by using equations derived from experimental data, such as the SIGMELTS algorithm (available online at http://calcul-isto.cnrs-orleans.fr/apps/sigmelts) of *Pommier and Le Trong* (2011), or other available melt resistivity equations, such as those of *Laumonier et al.*, 2017. Note that one must be careful to not exceed the solubility limits when choosing water content values (*Newman and Lowenstern,* 2002). The pressure is calculated from the depth, assuming a simple lithostatic relation (i.e., pressure = density·depth·g, g = 9.81 m/s^2; using 2800 g/m^3 for the crust and 3000 g/m^3 for the mantle, from *James et al.,* 2003). The resistivity of the rock matrix can be computed using the experimental resistivity-temperature relation of *Hashim et al.* (2013). For lower crustal depths ~37 km, assuming a temperature of 850°C, this relation gave a resistivity of 720 Ωm for the rock matrix.

The pure melt resistivity was predicted for a range of compositions and temperatures (**Figure S7a**) for ~37 km depth, using the SIGMELTS algorithm. A pure melt resistivity of 1.2 Ωm was calculated for 850°C, 1000 MPa (~37 km depth), and 6 wt% water content. Additionally, in this study the melt resistivity equation of *Laumonier et al.* (2017) was used. It had a fixed composition (andesite) and a much higher sensitivity to water content. It gave similar results to the SIGMELTS algorithm when a water content of 4.4 wt% was used. Both values remain in the possible range and do not significantly change the results.

Secondly, a two-phase equation was used to combine the resistivity of the pure melt and the rock matrix. This study used both the modified Archie's law (MAL) of *Glover et al.* (2000) and the Hashin-Shtrikman lower-resistivity bound (HL-LB) from *Hashin and Shtrikman* (1963). When the pure melt resistivity estimate is combined with the rock matrix resistivity the melt fraction needed to explain the observed bulk resistivity can be estimated. For lower crustal depths of ~37 km, 4.5% melt is required (**Figure S7b**). A range of 4 - 8.5% melt is calculated over the possible temperature range, with water content fixed at 6 wt%. The required melt fraction increases for a moderately interconnected melt geometry (m=1.5) to 12% melt (range 9 - 16%). It increases significantly to 18% melt (range 13 - 30%) for a lower water-content (1 wt%). For the lower crust, such high amounts of melt may be inconsistent with petrological evidence, and aqueous fluids are a much more likely explanation.
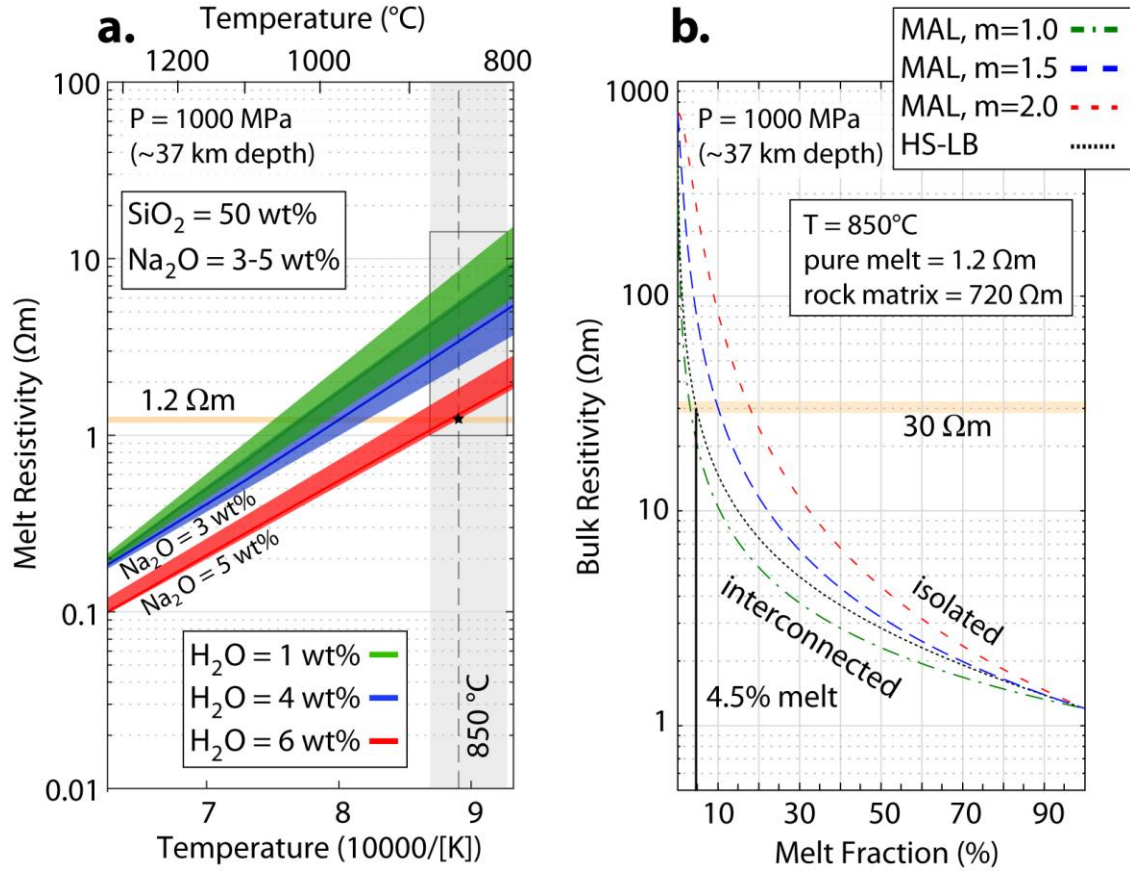
Figure S7: a: Variation of pure melt resistivity as a function of temperature for melts at ~37 km depth (pressure of ~1000 MPa) for a range of water contents (H_2O; 1 - 6 wt%, colours) and sodium contents (Na_2O; 3 - 5 wt%). The resistivity data were computed using the SIGMELTS algorithm of *Pommier and Le Trong* (2011). The range of all possible values are indicated by the gray box and the value taken to be typical is indicated by the star. The temperature estimates from thermobarometry of Hangai lavas are shown in grey (800 - 880 °C), with the typical temperature used in the calculations indicated with a dashed gray line. Using the typical temperature and a maximal water content gives a pure melt resistivity of ~1.2 Ωm (orange horizontal line). **b:** Bulk resistivity of a partially molten rock as a function of melt fraction. The resistivity of the rock matrix was computed using the resistivity-temperature relation of *Hashim et al.* (2013), which gave 720 Ωm for the rock matrix at a temperature of 850°C. Dashed lines show the bulk resistivity computed using the modified Archie's law (MAL) (*Glover et al.*, 2000) for various degrees of melt interconnection, from highly interconnected (m=1.0; green) and moderately-well interconnected (m=1.5; blue) to isolated (m=2.0; red). The dotted black line shows the Hashin-Shtrikman lower-resistivity bound (HS-LB) (*Hashin and Shtrikman*, 1963), which is the preferred value for interconnected melts. The approximate resistivity of the model anomaly C2 is ~30 Ωm, and this intersection gives the minimum melt fraction, 4.5%, required to fit the MT data. Typical value are shown here but the analysis was repeated for a range of possible values. If higher values of pure melt resistivity are used then a higher melt fraction is required.

9

Text S4. Enlarged 2-D model crustal section

An enlarged section of the resistivity model below the Hangai Dome (**Figure S8**) illustrates the crustal features. Upper crustal features such as C4 are interpreted as the electrical signatures of ancient magma conduits. F1 is interpreted as the South Hangai fault zone, which marks a significant terrane boundary. Hot springs locations are coincident with reduced near-surface resistivity.
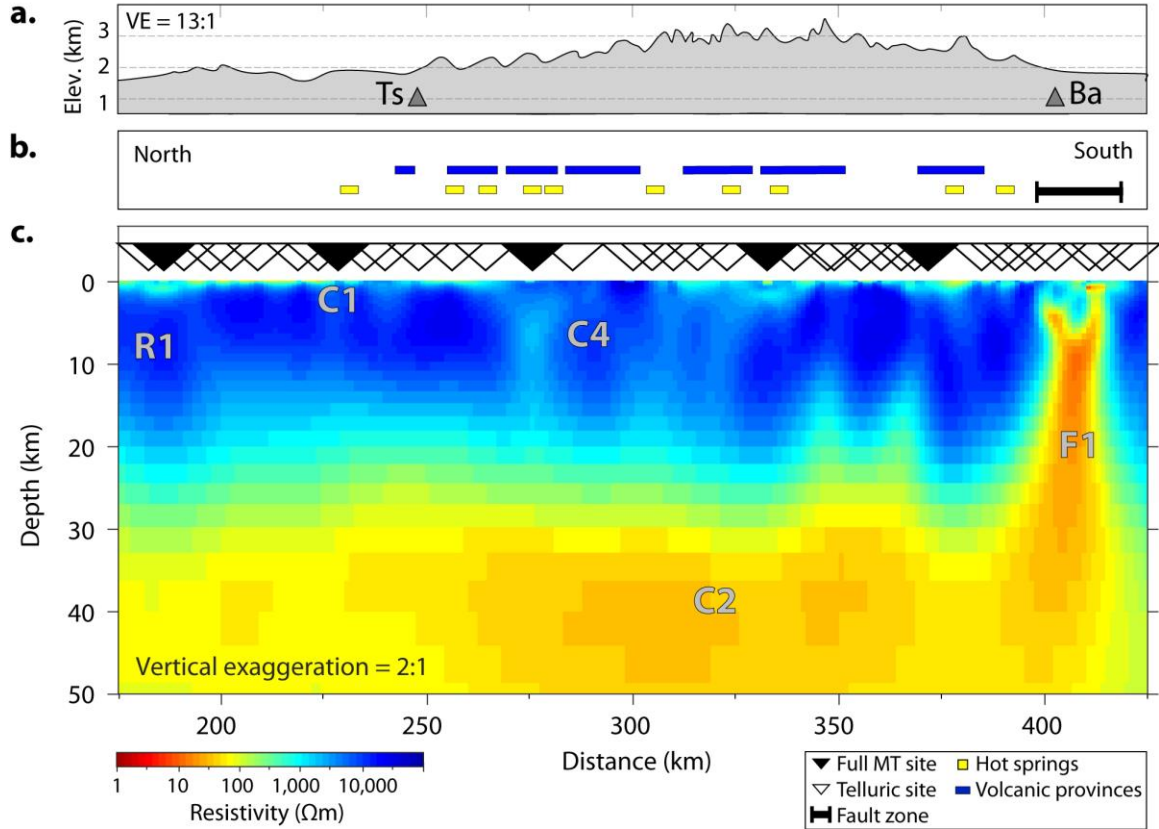

Figure S8: Resistivity model, as in Figure 3d, enlarged and with a vertical exaggeration of 2:1. **a:** Elevation along the profile. Ts = Tsetserleg; Ba = Bayankhongor. **b:** Additional information: volcanic provinces (blue) (*Sahagian et al.*, 2014; *Hunt et al.*, 2012); hot springs (gold) (*Ganbat and Demberel*, 2010); South Hangai fault zone (black) (*Walker et al.,* 2007; *Walker et al.,* 2008). **c:** The 2-D resistivity model obtained from the inversion of magnetotelluric data, as in Figure 3d.

Supplemental reference list

Booker, J., 2014, The Magnetotelluric Phase Tensor: A Critical Review: Surveys in Geophysics, v. 35, p. 7-40.

James, D.E., Niu, F., Rokoskyac, J., 2003, Crustal structure of the Kaapvaal craton and its significance for early crustal evolution: Lithos, v. 71, p. 413-429.